JOURNAL OF GEOPHYSICAL RESEARCH, VOL. 106, NO. C8, PAGES 16,917–16,928, AUGUST 15, 2001

Experiments on focusing unidirectional water waves

Michael G. Brown
Rosenstiel School of Marine and Atmospheric Science, University of Miami, Miami, Florida, USA

Atle Jensen
Mechanics Division, Department of Mathematics, University of Oslo, Oslo, Norway

Abstract. Results of four groups of experiments involving transient, mechanically generated water waves in a narrow wave tank are described. The purpose of these experiments was to investigate the limitations of the validity of linear theory predictions of the spatiotemporal structure of the surface elevation in focal regions. For unidirectional surface gravity waves, focusing occurs as a result of long waves overtaking short waves. Surprisingly, in our measurements, nonlinear effects are stronger in deep water than in intermediate depth water and are stronger in nonfocusing wave trains than in focusing wave trains. These trends can be explained by the observation that the dominant source of nonlinear interaction in our measurements was the Benjamin-Feir instability, which acts only over a limited duration in focusing wave trains, only in wave trains whose bandwidth is narrow, and only in deep water. Under conditions in which the Benjamin-Feir instability does not act (as is expected to be the case in the ocean), predictions that take into account amplitude-dependent dispersion but otherwise neglect nonlinear effects are in good agreement with measurements for wave trains with $(ka)_{\max}$ slightly in excess of 0.30.

1. Introduction

The work reported here was motivated by recent attempts [*Boccotti*, 1989, 1997; *Phillips et al*., 1993a, 1993b; *Pelinovsky and Kharif*, 2000; *Brown*, 2001] to describe the expected spatiotemporal structure of the sea surface in the vicinity of extreme wave events using linear theory. In these publications, extreme waves are modeled either as local maxima of a stationary Gaussian random process or as manifestations of space-time caustics where wave energy (or wave action, as appropriate) is locally focused. The details of these differing theoretical models of extreme waves are not important in the work reported here. Instead, we focus on a more fundamental question: does the linear theory description of water waves remain approximately valid in the vicinity of large wave events?

In view of the considerable effort that has been devoted to the study of finite amplitude water waves over the past few decades (see, e.g., the recent review by *Dias and Kharif* [1999]) the need for reexamining the limits of the validity of linear theory might be questioned. While it is clear that nonlinear effects play very important roles in the long-term evolution of ocean waves [see, e.g., *Komen et al*., 1994], near the onset of wave breaking [see, e.g., *Dommermuth et al*., 1988] and in other circumstances it is not clear that nonlinear effects necessarily play a critical role in the evolution of localized wave field features, even if the feature of interest is an anomalously large (but nonbreaking) wave. In this paper we seek to assess the bounds of validity of a local, in both space and time, linear theory description of water waves in the vicinity of focal events.

We present the results of four groups of experiments involving transient, mechanically generated water waves in a narrow wave tank. The experimental work was performed at the University of Oslo's Hydrodynamics Laboratory in a wave tank of width 51 cm, depth 1 m, and length 25 m. A programmable piston-driven hydraulic pump controlled one of the vertical end walls (the wave "paddle") of the tank to generate waves in a repeatable fashion. At selected fixed locations, resistance-type wave staffs measured the time histories of the waves that were generated. Absorbing material covering a "beach" extending over ~6 m at the opposite end of the wave tank effectively eliminated reflected waves. By generating waves whose period increased with increasing time a focal region (where longer waves overtake shorter waves) was produced near the center of the tank. *Rapp and Melville* [1990] have used essentially the same experimental setup to generate and study breaking waves. In our work, wave amplitudes were varied but, in all cases reported, were less than those that produced wave breaking. Wave amplitudes a were varied in the hope of establishing an approximate bound on wave steepness ka (where k is the horizontal wavenumber), below which linear theory is approximately valid. Our observations indicate that wave breaking occurs when the instantaneous local wave steepness $(ka)_{\max}$ exceeds ~0.44. With this in mind it should be noted that those measurements reported here for which $(ka)_{\max}$ is near or above 0.3 correspond to very steep waves that are not far from breaking. *Pierson et al*. [1992] have also experimentally investigated limitations of the linear theory description of steep nonbreaking surface gravity waves.

The remainder of this paper is organized as follows. In section 2, experimental results for four groups of experiments are presented. These results are presented in the order in which the experiments were performed. A brief rationale is given for performing each group of experiments. In section 3 a more quantitative description of how our linear theory wave field calculations were performed is presented. Included is a discussion of the effects of friction, surface tension, and finite amplitude dispersion. In section 4, measured wave spectra are

Copyright 2001 by the American Geophysical Union.

Paper number 2000JC000584.
0148-0227/01/2000JC000584$09.00

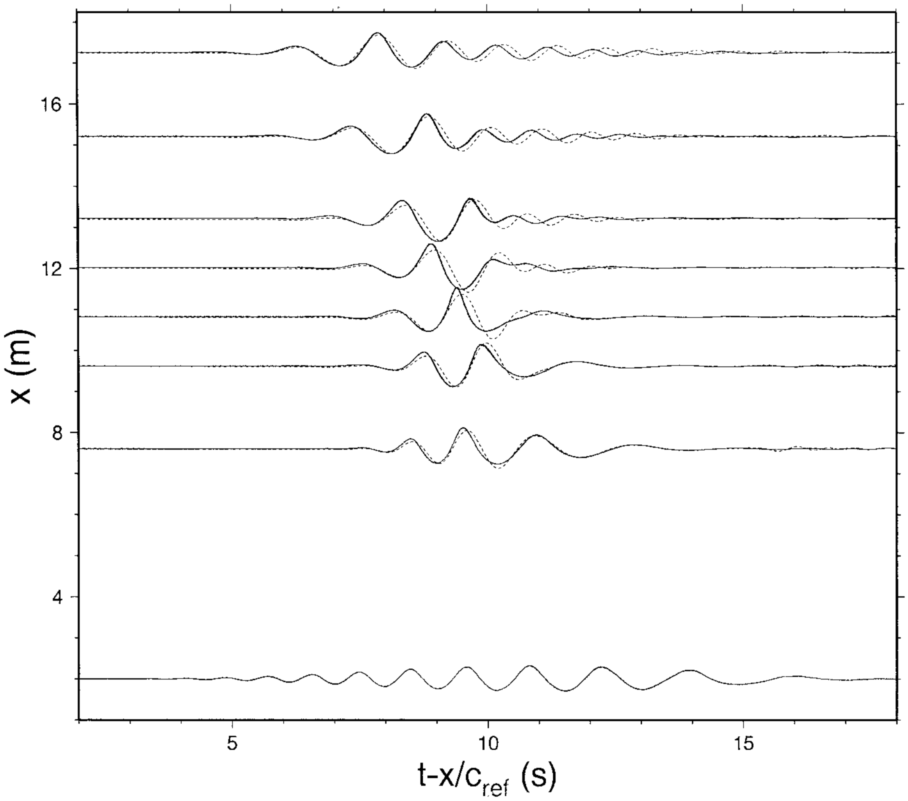

Figure 1. Group one wave measurements (solid lines) corresponding to $(ka)_{\max} = 0.35$ and linear theory–based predictions (dashed lines). The water depth is 60.0 cm, $c_{\text{ref}} = 1.0 \text{ m s}^{-1}$, and a distance of 1 m corresponds to a surface displacement of 16 cm.

presented and discussed. In section 5, the results are summarized and discussed.

2. Preliminary Description of Experimental Results

Figure 1 shows a subset of the data from the first group of experiments that was performed. In Figure 1 and in similar figures that follow, three measured sets of time histories are shown together with a single linear theory–based prediction. The manner by which the latter was constructed will be discussed in section 3. Differences in the three sets of measured time histories are not visible on the scale at which the data are plotted. Sets of measurements were made using four different values of peak paddle amplitude using the same paddle waveform. One such set is shown in Figure 1. This was done so that the validity of linear theory could be tested as a function of wave steepness ka. For the conditions shown in Figure 1, $(ka)_{\max} = 0.35$. The other group one measurements had $(ka)_{\max}$ values of 0.09, 0.24, and 0.40; waves in the latter set of measurements were very close to breaking. All reported measured values of $(ka)_{\max}$ in this paper are the maximum rate of change of the average (over three realizations) surface elevation $\partial\bar{\zeta}/\partial t$ divided by the wave phase speed at the measured spectral peak. (In this procedure the phase speed at the spectral peak is an approximation to the instantaneous phase speed at the maximum of $\partial\bar{\zeta}/\partial t$. In our experiments this approximation is expected to be very good as can be seen by comparing wave train time histories and the corresponding space-time ray plots. In principle, the instantaneous phase speed is computable as the rate of change of the phase of the Hilbert transform envelope of $\bar{\zeta}(t)$.)

For the data set shown in Figure 1 the water depth was $h = 60.0$ cm, and the paddle input voltage time history had the form

$$V(t) = b(t) \sin \phi(t) \tag{1}$$

for $0 \leq t \leq t_s$ with

$$b(t) = \frac{256}{27} \frac{t^3(t_s - t)}{t_s^4} V_m \tag{2}$$

$$\phi(t) = 2\pi f_o t\left(1 - \alpha \frac{t}{t_s}\right). \tag{3}$$

Here V_m, the voltage maximum, was variable, $t_s = 18$ s, $f_o = 1.5$ Hz, and $\alpha = 0.4$. Corresponding to (1)–(3), the instantaneous wave frequency at the wall is approximately

$$\omega(t) = \frac{d\phi}{dt} = 2\pi f_o\left(1 - 2\alpha \frac{t}{t_s}\right). \tag{4}$$

From this expression a set of space-time rays (see Figure 2) can be constructed. Each space-time ray corresponds to a surface of constant ω (because the environment is time-invariant) whose slope, $dx/dt = \partial\omega/\partial k$, is constant (because the water depth is not a function of position). These conditions define the slope and $x = 0$ intercept of each line (ray) plotted in Figure 2. It is straightforward to verify that under deep water

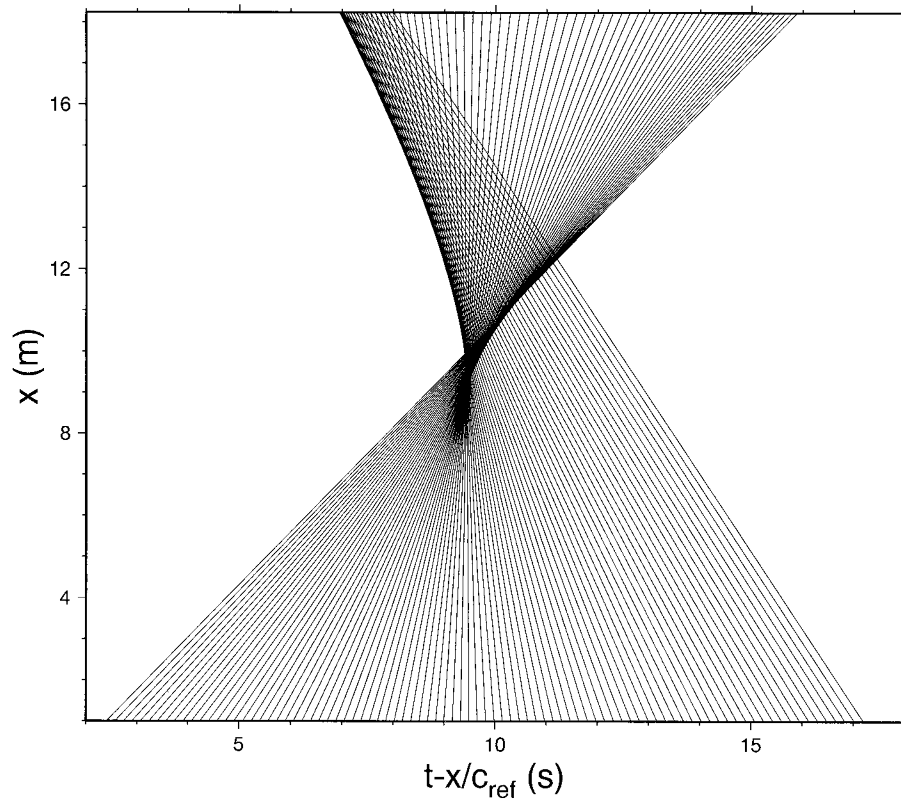

Figure 2. Space-time ray diagram corresponding to the wave field shown in Figure 1.

conditions, the simple FM sweep defined by (4) produces a perfect focus at

$$x_f = \frac{g t_s}{8\pi\alpha f_o}. \tag{5}$$

For the parameters chosen, $x_f = 11.7$ m. A perfect focus is not seen, even approximately, in Figure 2 because the lower-frequency waves that were generated do not satisfy the deep water dispersion relation. (When calculating the slope of each ray, corrections, discussed in section 3, to the dispersion relation to account for frictional boundary layers and finite amplitude dispersion were not taken into account.)

The interpretation of (4) as wave frequency at the wall assumes that the amplitude $b(t)$ (equation (2)) is a slowly varying function and does not take into account the input voltage to paddle displacement transfer function or nonlinear effects in the coupling between the wave paddle and the waves. We emphasize that these approximations affect only our space-time ray plots, which we regard merely as qualitative guides to aid in the interpretation of our experimental results. Our linear theory–based wave field calculations do not require that any of these assumptions be made; these calculations will be discussed in the section 3.

As expected, agreement between measurements and linear theory predictions degraded with increasing $(ka)_{\max}$. (This dependence is shown in Figure 9, which will be discussed in more detail below.) Agreement was good for $(ka)_{\max} = 0.24$ but was noticeably degraded for $(ka)_{\max} = 0.35$ (see Figure 1). A factor that was thought to contribute to the linear theory prediction errors in these experiments was that these experiments were performed in intermediate depth water ($0.5 \lesssim kh \lesssim 5.4$). Our expectation was that nonlinear effects would be weaker in deep water. To test this expectation, it was decided to make a similar set of measurements using a combination of deeper water and higher wave frequencies.

A representative set of results for the second group of experiments is shown in Figure 3. The water depth was 79.7 cm. The wave paddle input voltage was again described by (1)–(3), this time with $t_s = 18.0$ s, $f_o = 2.0$ Hz, and $\alpha = 0.3$, again corresponding to $x_f = 11.7$ m. The corresponding space-time rays are shown in Figure 4. Because deep water conditions are nearly satisfied ($2.1 \lesssim kh \lesssim 12.9$), only slight deviations (at the lowest frequencies) from a perfect focus are seen in the ray diagram. Again, four values of the peak input voltage were used so that the validity of linear theory as a function of ka could be tested. Figure 3 corresponds to moderately steep waves with $(ka)_{\max} = 0.23$. The other group two measurements had $(ka)_{\max}$ values of 0.12, 0.16, and 0.28.

Again, agreement between measurements and linear theory predictions degraded with increasing $(ka)_{\max}$. Agreement was good for $(ka)_{\max} = 0.12$ but was noticeably degraded for $(ka)_{\max} = 0.23$ (see Figure 3). This trend is not surprising. It is surprising, however, that for comparable values of $(ka)_{\max}$, linear theory performed better in the (intermediate depth) group one experiments than in the (deep water) group two experiments. A possible explanation for this behavior is that the near-perfect focus in the group two experiments presented a particularly difficult challenge for linear theory. To test whether this was the case, a third set of experiments was performed using a slightly modified paddle waveform.

A representative set of results from the third group of experiments is shown in Figure 5. The corresponding rays are shown in Figure 6. For this group of experiments the paddle input voltage had the form (1) and (2) with

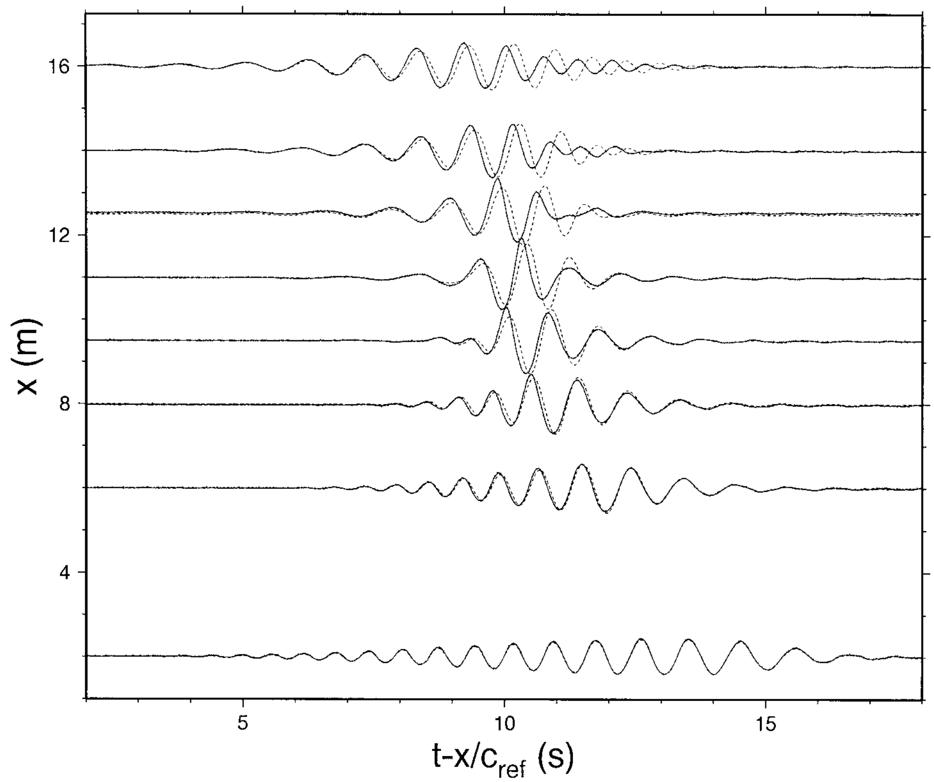

Figure 3. Group two wave measurements (solid lines) corresponding to $(ka)_{\max} = 0.23$ and linear theory–based predictions (dashed lines). The water depth is 79.7 cm, $c_{\mathrm{ref}} = 0.6$ m s^{-1}, and a distance of 1 m corresponds to a surface displacement of 4 cm.

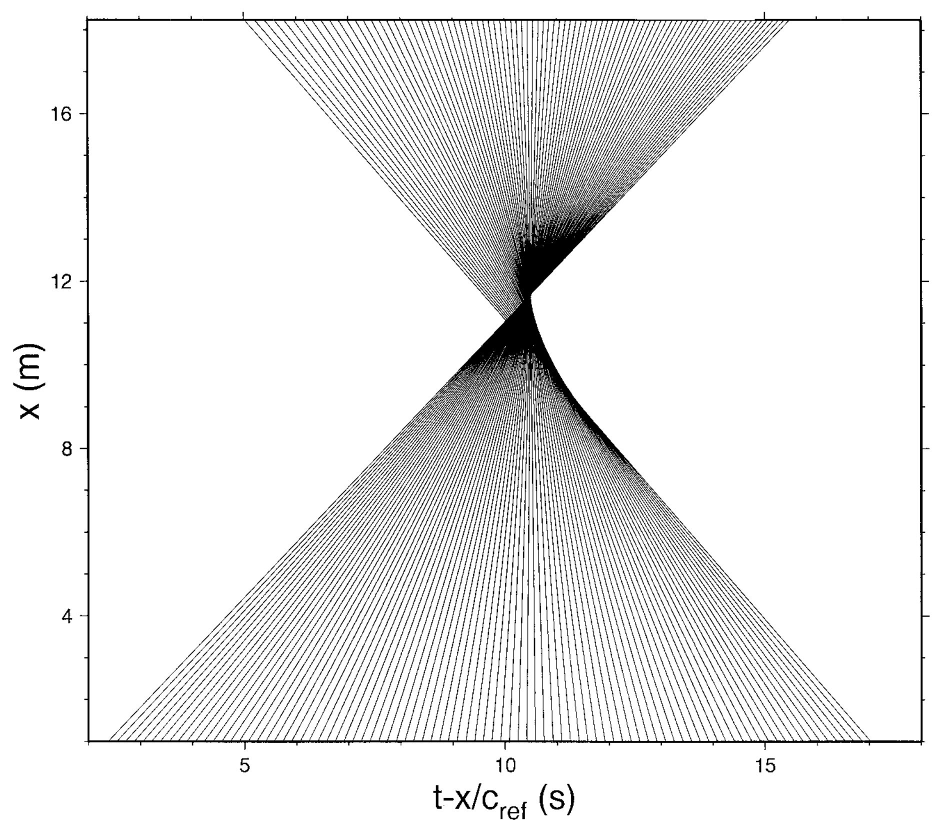

Figure 4. Space-time ray diagram corresponding to the wave field shown in Figure 3.

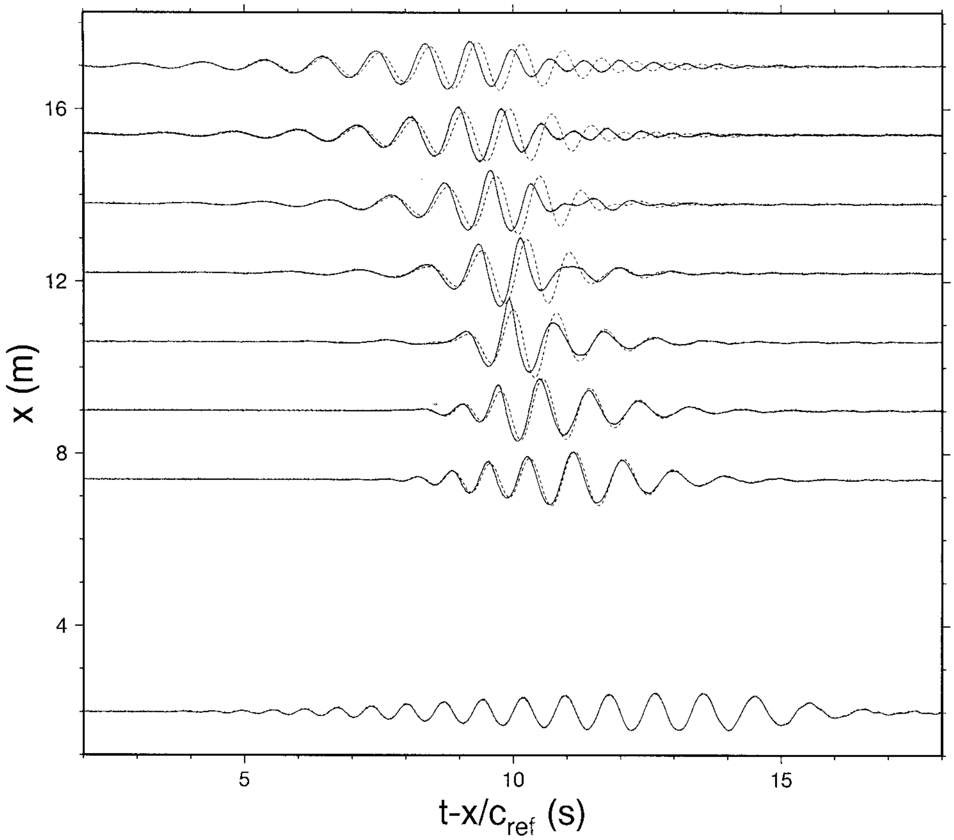

Figure 5. Group three wave measurements (solid lines) corresponding to $(ka)_{\max} = 0.22$ and linear theory–based predictions (dashed lines). The water depth is 60.0 cm, $c_{\mathrm{ref}} = 0.6$ m s^{-1}, and a distance of 1 m corresponds to a surface displacement of 4 cm.

$$\phi(t) = 2\pi f_o t\left[\left(1 - \alpha \frac{t}{t_s}\right) - \frac{\beta t_s}{3\pi}\cos\left(3\pi \frac{t}{t_s}\right)\right]. \quad (6)$$

The source function parameters were $t_s = 18.0$ s, $f_o = 2.0$ Hz, $\alpha = 0.3$, and $\beta = 0.015$, and the water depth was $h = 60.0$ cm, corresponding to $1.7 \lesssim kh \lesssim 9.7$. Again, four values of the peak input voltage were used. The results shown in Figure 5 correspond to waves with $(ka)_{\max} = 0.22$. The other group three measurements had $(ka)_{\max}$ values of 0.13, 0.17, and 0.30. The perturbation term in the phase function (6) (compare to (3)) was chosen so that the caustic structure seen in Figure 4 (almost a perfect focus) would unfold into a section of a generic low-order space-time caustic [see *Brown*, 2001]. The caustic structure seen in Figure 6 is a section of a "swallowtail," which satisfies the stated objective. Other forms of the phase function (6) could have been used to generate a wave field whose caustic structure is topologically equivalent to that shown in Figure 6.

Again, agreement between measurements and linear theory predictions degraded with increasing $(ka)_{\max}$. Agreement was good for $(ka)_{\max} = 0.13$ but was noticeably degraded for $(ka)_{\max} = 0.22$ (see Figure 5). This behavior is essentially the same as that observed in the group two experiments; compare, for example, Figures 3 and 5. This suggests that in deep water, nonlinear effects are not strongly influenced by details of how the waves are focused. To provide a baseline against which these results could be compared, it was decided to investigate the behavior of a nonfocusing wave train in deep water.

The input waveform used in the fourth and final group of experiments is described by (1)–(3) with $t_s = 18.0$ s, $f_o = 1.5$ Hz, and $\alpha = 0$ with a water depth of $h = 59.4$ cm; $kh \approx 5.4$ for this nearly monochromatic wave train. Four sets of measurements, corresponding to $(ka)_{\max}$ values of 0.15, 0.19, 0.25, and 0.44, were made. The highest wave in the last set of experiments broke about 1 m beyond the most distant measurement location (at which $(ka)_{\max} = 0.44$ was observed). The measurements corresponding to $(ka)_{\max} = 0.25$ are shown in Figure 7. The corresponding space-time ray diagram is shown in Figure 8. Note that the $\alpha \to 0$ limit of (5) applies so $x_f \to \infty$. Surprisingly, in this nonfocusing limit the agreement between measurements and linear theory predictions for comparable values of $(ka)_{\max}$ is somewhat worse than was the case in the groups two and three experiments where focusing was present.

The results described in this section are surprising for two reasons: (1) the agreement between linear theory predictions and measurements is better in intermediate depth water than in deep water, and (2) the agreement between linear theory predictions and measurements in deep water is better for focusing wave trains than for nonfocusing wave trains. After a digression to explain how our linear theory predictions were constructed we will return our attention to explaining these surprising trends. To reduce the number of figures somewhat, we shall hereafter display results only for the group one, three, and four experiments. Results for the group two experiments are very similar to those for the group three experiments. This is not surprising inasmuch as both involve focusing waves in deep water.

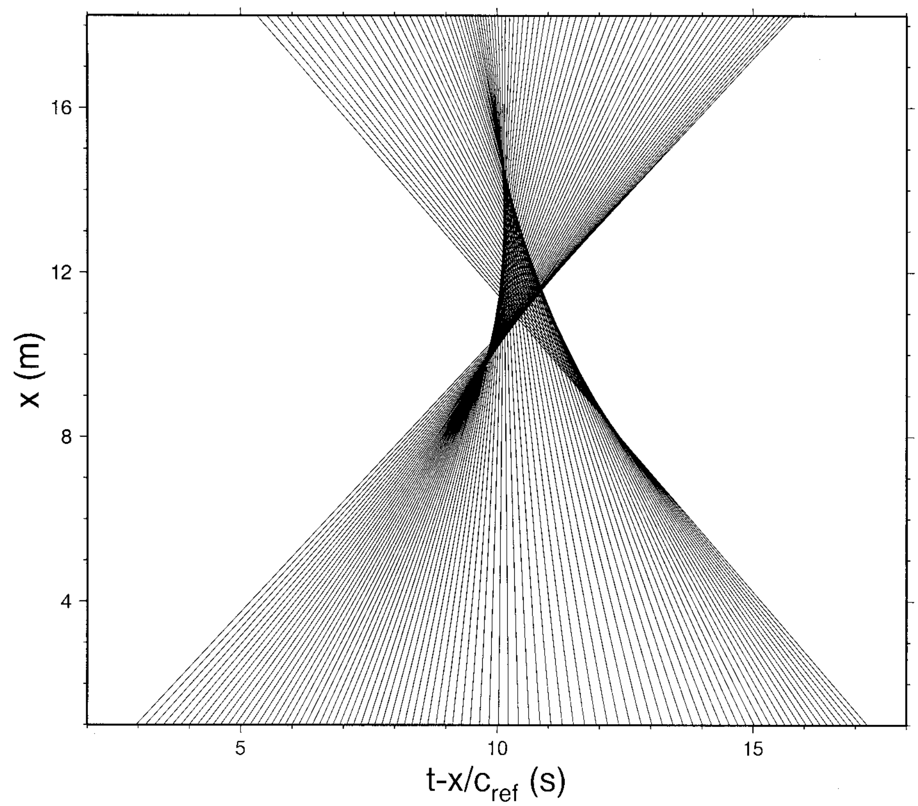

Figure 6. Space-time ray diagram corresponding to the wave field shown in Figure 5.

3. Linear Theory Calculations

The linear theory solution to the wave maker problem (compute the surface displacement $\zeta(x, t)$ from a knowledge of the wall displacement $d(t)$) was first described by *Kennard* [1949]. Unfortunately, this solution is singular at the point where the free surface touches the wall (D. H. Peregrine, unpublished manuscript, 1972). The extent to which this flaw of the linear solution to the wave maker problem affects the solution at distant points is not known. In addition to this problem, one expects that nonlinear coupling effects between the moving wall and the water will be present, independent of the presence or absence of finite amplitude wave propagation effects at distant points in the wave tank. In our study it is highly desirable to eliminate nonlinear coupling effects between the wave paddle and the water so that finite amplitude wave propagation effects can be isolated. With these comments in mind the technique described below was used to construct linear theory wave field predictions.

The general linear theory solution has the form of a Fourier integral. For unidirectional waves the usual Fourier integral solution to the initial value problem has the form of an integral over wavenumber k. For our purposes it is convenient to make a change of variables from k to ω; because $\partial\omega/\partial k \neq 0$, there is no loss of generality in doing so. The resulting Fourier integral representation of the free surface displacement can be written

$$\zeta(x, t) = \int_{-\infty}^{\infty} A(\omega) e^{i[k(\omega)(x-x_o)-\omega t]}\, d\omega, \tag{7}$$

where

$$A(\omega) = \frac{1}{2\pi}\int_{-\infty}^{\infty} \zeta(x_o, t) e^{i\omega t}\, dt. \tag{8}$$

After computing $A(\omega)$ using (8), ζ can be computed for all t at those x values of interest using (7). (For numerical purposes, (7) and (8) were replaced by their discrete Fourier transform counterparts and were evaluated using fast Fourier transforms (FFTs).) Experimentally, the reference position x_o was taken to be 2 m in front of the wave paddle. Use of this procedure eliminates nonlinear coupling effects that may be present in the vicinity of the wave paddle (somewhat arbitrarily taken to be $x < 2$ m) at the cost of reducing the number of available wave sensors by one and effectively shortening the wave tank by 2 m. Because of the trancendental nature of the surface gravity wave dispersion relation,

$$\omega^2 = gk \tanh(kh), \tag{9}$$

the function $k = k(\omega)$ was constructed using a table look up and interpolation procedure. The linear theory wave field predictions shown in Figures 1, 3, 5, and 7 were computed using (7) and (8) with $k(\omega)$ defined by (9).

Examination of Figures 1, 3, 5, and 7 shows that the principal shortcoming of the linear theory predictions is that the linear theory phase is retarded (phase speeds too small) relative to the measurements. The effects of surface tension, frictional boundary layers, and finite amplitude dispersion produce measurable phase perturbations that have not yet been accounted for. Surface tension increases phase speeds, while frictional boundary layers [see *Mei and Liu*, 1973] reduce phase speeds. Both effects are small in our experiments. Furthermore, the

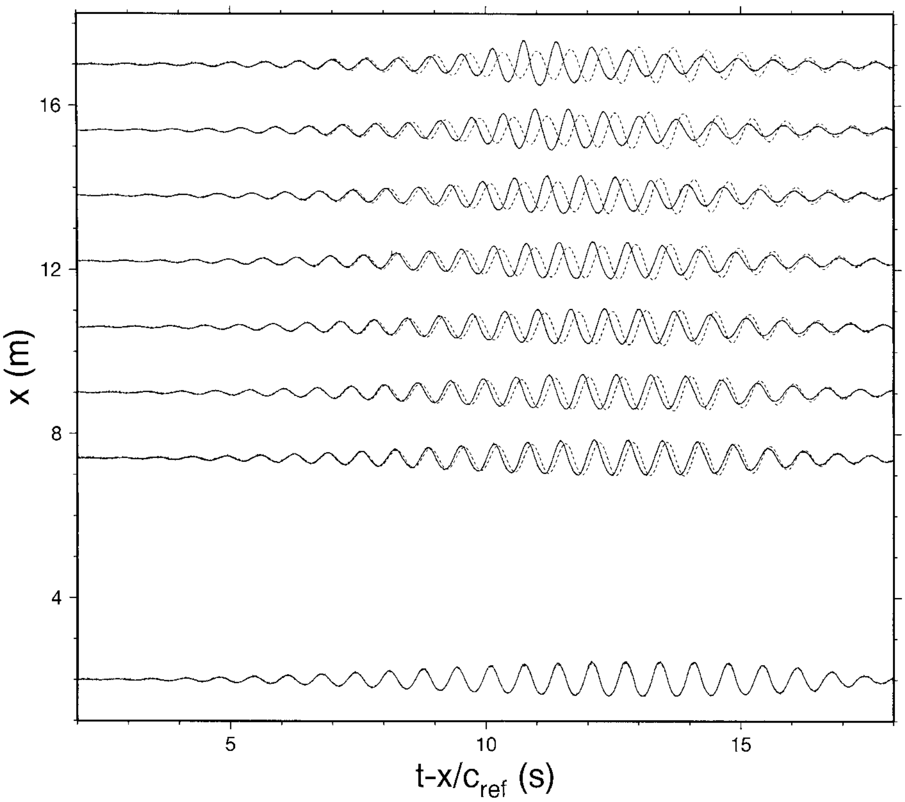

Figure 7. Group four wave measurements (solid lines) corresponding to $(ka)_{\max} = 0.25$ and linear theory–based predictions (dashed lines). The water depth is 59.4 cm, $c_{\mathrm{ref}} = 0.594 \text{ m s}^{-1}$, and a distance of 1 m corresponds to a surface displacement of 4 cm.

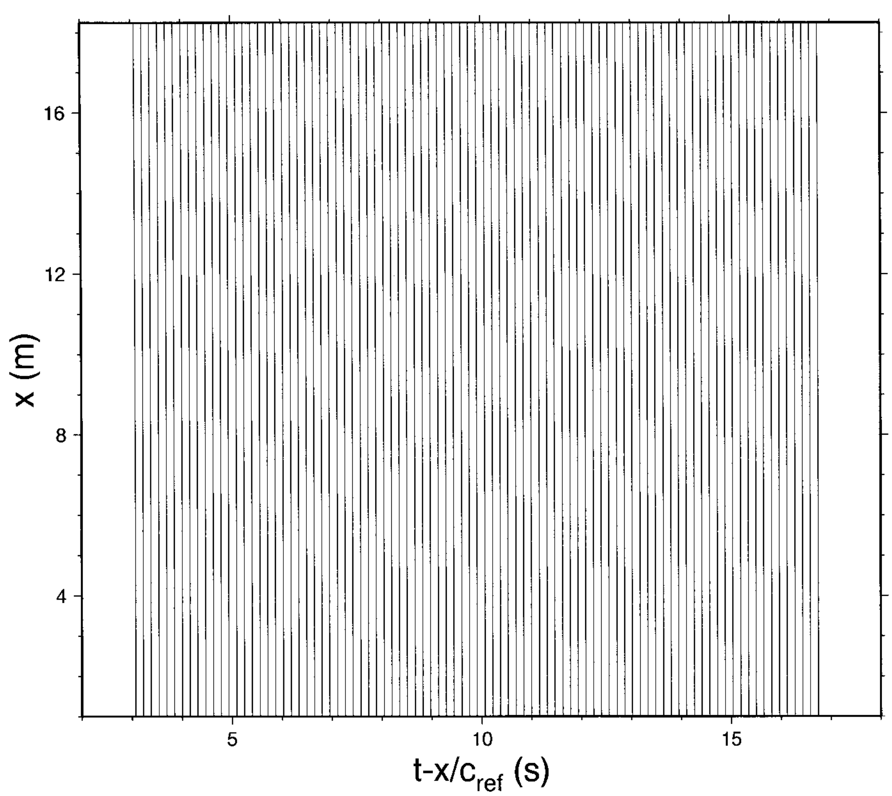

Figure 8. Space-time ray diagram corresponding to the wave field shown in Figure 7.

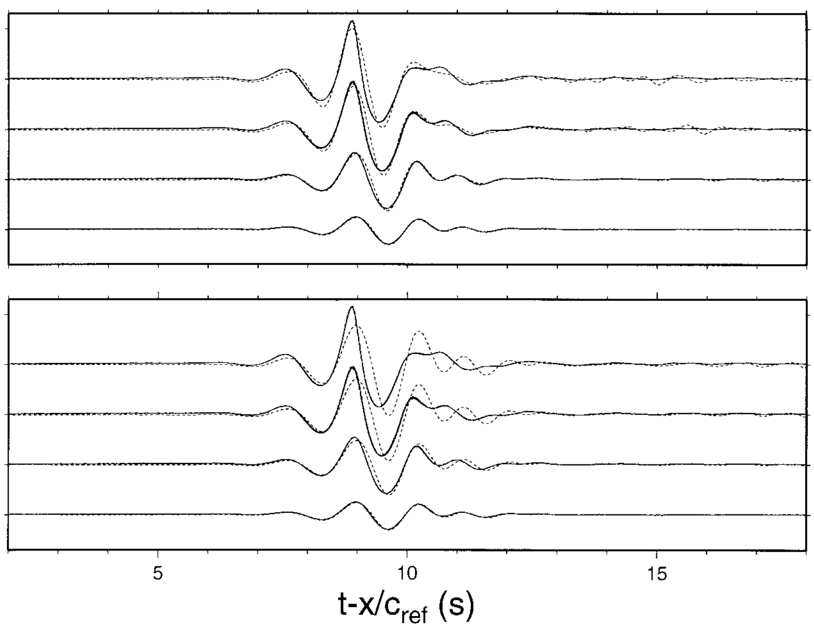

Figure 9. Group one wave measurements (solid lines) and predictions (dashed lines) at a fixed location, $x = 12.03$ m, for four different values of $ka_{\max}$: (bottom) linear theory– and (top) quasilinear theory–based predictions. The measurements shown have estimated $ka_{\max}$ values of 0.09, 0.24, 0.35, and 0.40, increasing upward. The water depth is 60.0 cm, $c_{\mathrm{ref}} = 1.0$ m s^{-1}, and the distance between tick marks in the vertical direction corresponds to a surface displacement of 16 cm.

phase corrections that result from these effects partially cancel. Finite amplitude corrections to the dispersion relation (9) lead to an increase in phase speeds. For the wavenumbers used in our experiments this effect is larger than the effects of both surface tension and frictional boundary layers provided wave amplitudes are greater than about 5 mm. Also, phase differences between measurements and linear theory predictions were observed to increase with increasing wave amplitude; this strongly suggests that finite amplitude dispersion is the dominant cause of the misfit.

The lowest-order finite amplitude correction to the finite depth dispersion relation (9) is [see, e.g., *Whitham*, 1974]

$$\omega^2 = gk \tanh(kh) \cdot \left[1 + \left(\frac{9 \tanh^4 kh - 10 \tanh^2 kh + 9}{8 \tanh^4 kh}\right) k^2 a^2\right], \qquad (10)$$

where a is the wave amplitude. To invert (10) for $k = k(\omega)$, $a = a(k)$ on the right-hand side must be known. To account for the asymmetry of the measured wave spectra, $a = a(k)$ was approximated as two one-sided Gaussian distributions, which smoothly match at the spectral peak. After making this substitution, (10) was inverted using a table look up and interpolation procedure. Using this $k(\omega)$, wave fields can be computed using (7) and (8). We shall refer to wave field calculations of this type as quasilinear. In these calculations, finite amplitude dispersion is accounted for, but there is no exchange of energy between different spectral components of the wave field.

In Figure 9, group one wave measurements at a fixed location, $x = 12.03$ m, for a range of $(ka)_{\max}$ values are compared to both linear and quasilinear wave field predictions. Agreement between both types of prediction and measurements is seen to be better for smaller values of $(ka)_{\max}$, as expected. For all $(ka)_{\max}$ values the agreement between the energetic portion of the measurements and quasilinear predictions is seen to be better than the agreement between measurements and linear theory predictions. Figure 9 also shows, for the larger $(ka)_{\max}$ values, late arriving relatively high frequency energy in both the linear and quasilinear predictions that is not seen in the measurements. We attribute this shortcoming of our predictions to the presence of high-frequency energy that is phase-locked to longer (and hence faster) waves but which is erroneously treated as freely propagating wave energy in our simple predictions. In spite of this caveat, Figure 9 shows that for the group one measurements, there is fair agreement between measurements and quasilinear predictions, even for $(ka)_{\max} = 0.40$. This is somewhat surprising inasmuch as breaking was observed for estimated $(ka)_{\max}$ values in excess of 0.44.

Figures 10, 11, and 12 show a comparison between quasilinear wavefield predictions and measurements at all measurement locations for the same set of measurements that are shown in Figures 1, 5, and 7. Consistent with Figure 9, a comparison of Figures 10, 11, and 12 to Figures 1, 5, and 7, respectively, shows that quasilinear wave field predictions are in better agreement with measurements than are strict linear theory predictions. As expected on the basis of (10), quasilinear corrections to strict linear theory are observed to be larger in intermediate depth water than in deep water. For the group one experiments (involving focusing waves in intermediate depth water), good agreement between quasilinear predictions and measurements was found for $(ka)_{\max} \lesssim 0.33$; the $(ka)_{\max}$ value used in Figure 10 is near this approximate upper limit. For the groups two and three experiments (involving focusing waves in deep water), quasilinear predictions were found to be in good agreement with measurements for $(ka)_{\max} \lesssim 0.18$; the $(ka)_{\max}$ value used in Figure 11 lies outside of this

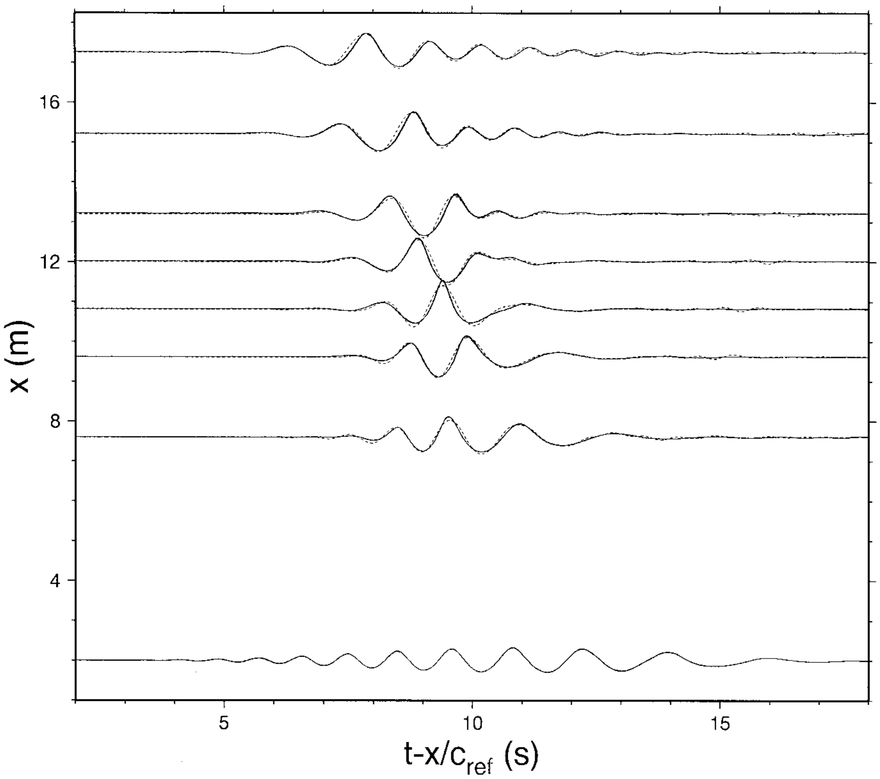

Figure 10. Same as Figure 1 except that quasilinear theory–based predictions are shown (dashed lines).

range. For the group four measurements (involving nonfocusing waves in deep water), quasilinear predictions were found to be in good agreement with measurements for $(ka)_{\max} \lesssim 0.15$; the $(ka)_{\max}$ value used in Figure 12 lies well outside of this range. (We have intentionally chosen to show examples for which differences between predictions and measurements can be seen. For smaller wave amplitudes, differences between predictions and measurements are no

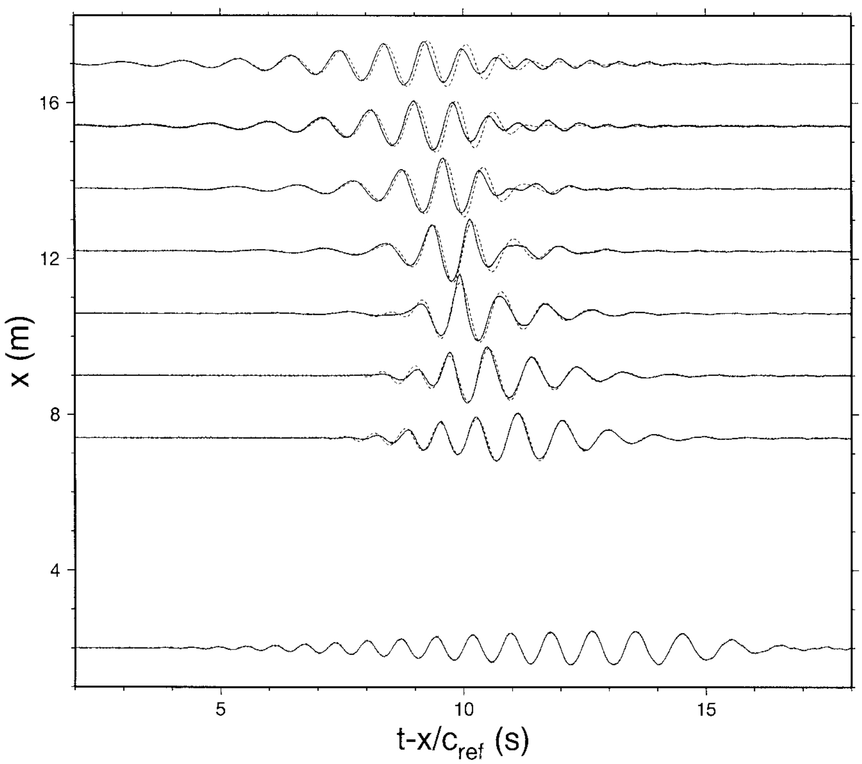

Figure 11. Same as Figure 5 except that quasilinear theory–based predictions are shown (dashed lines).

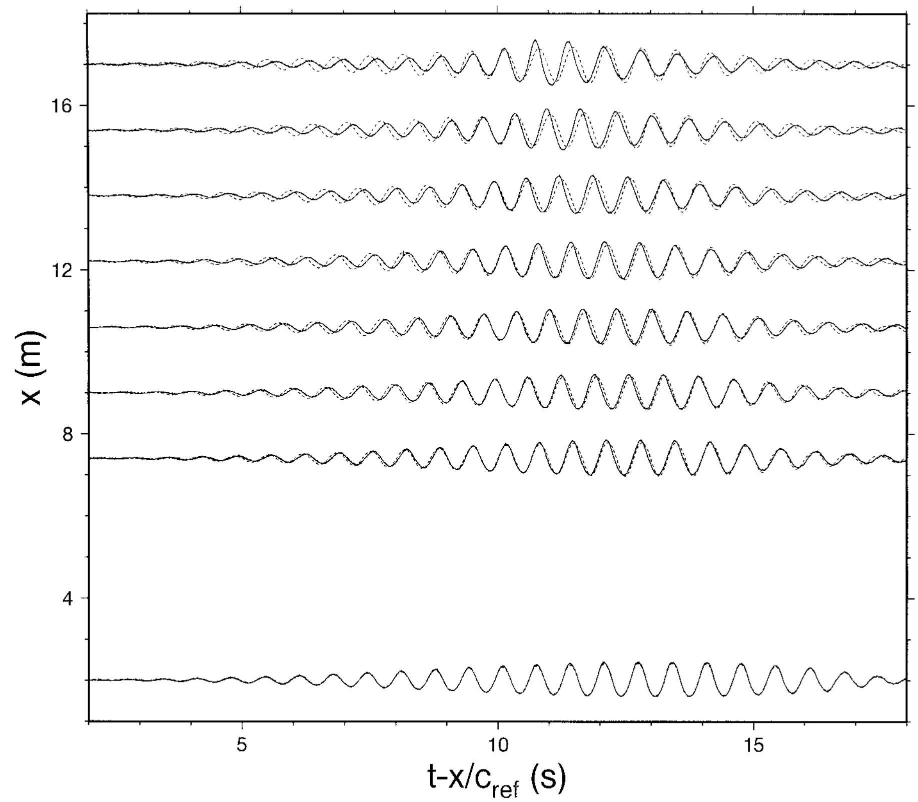

Figure 12. Same as Figure 7 except that quasilinear theory–based predictions are shown (dashed lines).

larger than differences between the three sets of measurements; the corresponding plots are uninteresting.)

We do not attach much significance to the values of the upper bounds on $(ka)_{\max}$ just quoted. It is significant, however, that the approximate upper bound on $(ka)_{\max}$ is greater for focusing waves in intermediate depth water than in deep water and that the approximate upper bound on $(ka)_{\max}$ is slightly greater for focusing waves than for nonfocusing waves in deep water. Thus the puzzling trends noted at the end of section 2 cannot be accounted for by finite amplitude dispersion.

4. Wave Spectra

Insight into the cause of the failure of linear theory can be obtained by examining the evolution of wave spectra. Normalized spectral difference plots are shown in Figures 13, 14, and 15; these correspond to the measurements shown in Figures 1 and 10, 5 and 11, and 7 and 12, respectively. Spectral differences are plotted because these show more clearly small changes in spectral shape. In these plots, $S_x(f)$ is the measured frequency power spectrum at position x, and $S_o(f)$ is the power spectrum measured at $x = x_o$ weighted by exp $[-2k_I'(\omega)(x - x_o)]$, where $k_I'(\omega)$ is the imaginary part of the complex wavenumber [see *Mei and Liu*, 1973]

$$k' = k\left[1 + (1+i)\frac{\delta}{b}\left(\frac{2kb + \sinh 2kh}{2kh + \sinh 2kh}\right)\right]. \quad (11)$$

The factor exp $[-2k_I'(\omega)(x - x_o)]$ accounts for energy losses in frictional boundary layers. In (11), $2b$ is the width of the wave tank, and $\delta = (\nu/2\omega)^{1/2}$ is the boundary layer thickness where ν is the kinematic viscosity of water. Each spectral estimate plotted in Figures 13, 14, and 15 is the average of nine independent spectral estimates; spectra from three sets of measurements were averaged, followed by averaging over three neighboring frequency bins.

Consider first Figure 15, corresponding to nonfocusing waves in deep water. Here energy is seen to be transferred from the spectral peak to sidebands. The cause of this behavior is the sideband instability described originally by *Benjamin and Feir* [1967]. In this instability the most unstable sidebands are predicted to have frequencies $\omega_o(1 \pm ka)$ whose energies are predicted to grow asymptotically like exp $(k^2a^2\omega_o t)$. Here ω_o

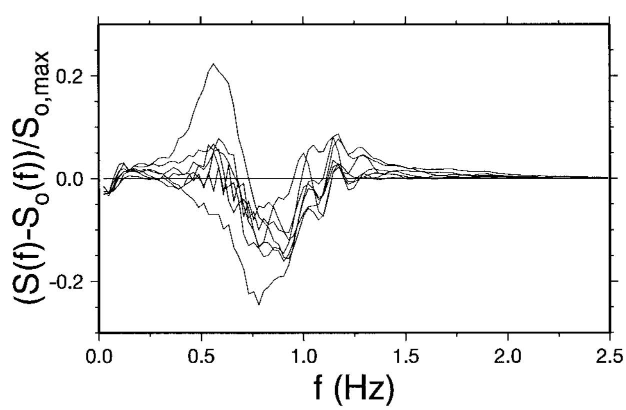

Figure 13. Normalized spectral differences corresponding to the measurements shown in Figures 1 and 10. The anomalously large negative and positive spectral differences correspond to the measurements at $x = 10.83$ m and $x = 13.22$ m, respectively.

is the center frequency of a wave train whose bandwidth is assumed to be narrow. These properties are in good agreement with Figure 14 for $ka = 0.08$. For the same set of measurements, estimates of $(ka)_{max}$ decrease from 0.20 at the reference location to 0.18 at the fourth record and then increase to 0.25 at the final record. A typical value of ka for the initial wave train is somewhat less than these estimates of $(ka)_{max}$, approximately twice the estimate, $ka = 0.08$, derived from Figure 15, as just described. This factor of 2 agreement is close enough that we feel that it supports our interpretation that the Benjamin-Feir instability is the cause of the spectral shifts seen in Figure 15.

Consider now Figure 14, corresponding to focusing waves in deep water. During the focusing phase of wave train evolution, which is isolated in Figure 14 (top), the spectral peak is seen to lose energy to sidebands, again suggesting that the Benjamin-Feir instability is acting. The location of the maximally unstable lower sideband and the growth rate of both sidebands are consistent with the above expressions using $ka = 0.18$. This value is intermediate between our estimates of $(ka)_{max}$, which fall between 0.12 and 0.22, in the corresponding time histories. Thus, again, there is some quantitative evidence suggesting that the Benjamin-Feir instability is acting. Note, however, that in the case of Figure 14 this evidence is based on a very small number of measurements. Also, it should be noted that the location of the maximally unstable upper sideband is not well defined in Figure 14. Some caveats are expected inasmuch as the corresponding wave initial conditions only crudely approximate the idealized conditions on which the Benjamin-Feir analysis is based. In spite of these caveats the aforementioned properties of Figure 14 (top) support the notion that during the focusing phase of wave train evolution the Benjamin-Feir instability is the dominant cause of nonlinear interactions. Figure 14 (bottom) suggests that the sideband instability that acts during the focusing phase of wave field evolution is effectively turned off during the defocusing phase. A heuristic explanation for this behavior will be given below.

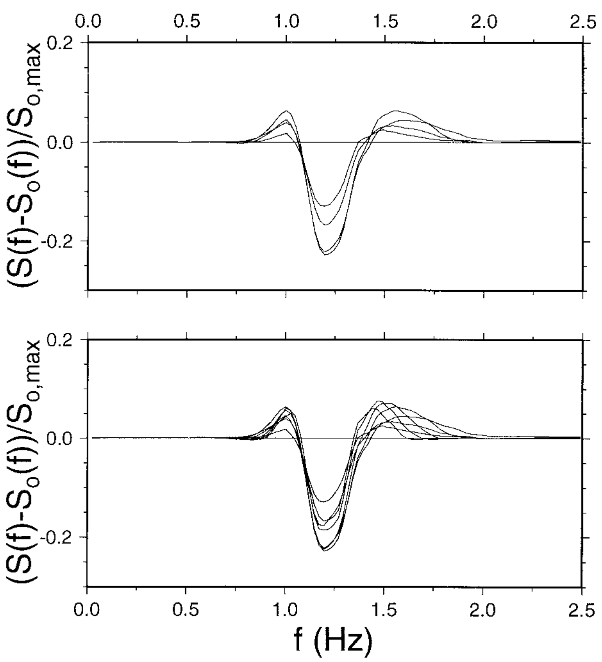

Figure 14. Normalized spectral differences corresponding to the measurements shown in Figures 5 and 11: (top) spectral differences at the first five measurement locations only, including the reference measurement, and (bottom) spectral differences at all eight measurement locations. As propagation distance increases, the minimum normalized spectral differences are 0.0 (at the reference measurement), −0.13, −0.17, −0.22, −0.23, −0.22, −0.19, and −0.18. Only in Figure 14 (top) do the magnitudes of the normalized spectral differences increase monotonically as a function of distance from the reference measurement location.

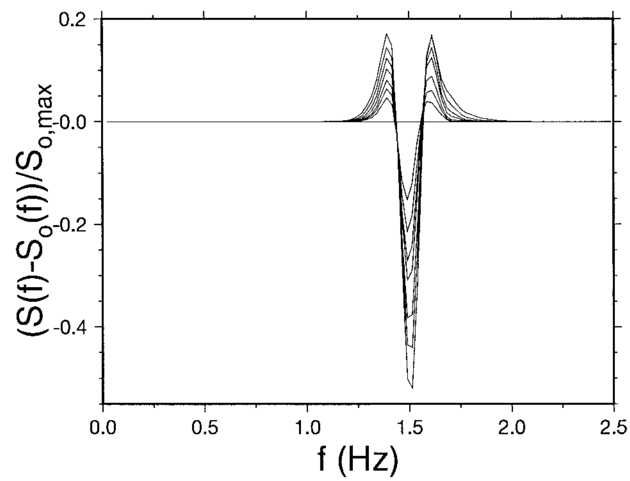

Figure 15. Normalized spectral differences corresponding to the measurements shown in Figures 7 and 12. The magnitudes of the normalized spectral differences increase monotonically as a function of distance from the reference measurement location.

Spectral differences corresponding to focusing waves in intermediate depth water are shown in Figure 13. There is no identifiable trend in Figure 13. We attribute most of the variability seen in Figure 13 to uncertainty in the spectral estimates. (The spectra corresponding to the group one measurements are more noisy than those for the groups two, three, and four experiments. This noise is, of course, amplified when differences are taken.)

The Benjamin-Feir instability is a deep water instability that acts only on essentially unidirectional wave trains whose bandwidth is narrow. *Alber* [1978] has derived a condition, that the wave train's bandwidth divided by its center frequency not exceed the average wave steepness, under which the Benjamin-Feir instability is able to act on a unidirectional wave train. This condition was easily satisfied in our group four experiments, was marginally satisfied in our groups two and three experiments, and was not satisfied in our group one experiments. In our group one experiments the Benjamin-Feir instability was unable to act both because the deep water condition was not satisfied and because Alber's bandwidth condition was not satisfied. (In these experiments, $kh \approx 1.3$ at the spectral peak and $\Delta f/f_{peak}$ was in excess of unity.) The absence of this instability in the group one experiments explains why linear theory wave field predictions were in better agreement with measurements for this group of experiments than for the groups two, three, and four experiments.

Our surprising observation that nonlinear effects were stronger in nonfocusing (group four) wave trains than in focusing (groups two and three) wave trains has also been observed in numerical simulations [*Henderson et al.*, 1999]. This behavior might be anticipated in view of Alber's bandwidth condition for applicability of the Benjamin-Feir instability; this condition was marginally satisfied in the groups two and three experiments but was easily satisfied in the group four experiments. The evolution of wave spectra shown in Figure 14 suggests the following slightly more complicated, albeit heuristic, explanation for this behavior. In the evolution of a focusing wave train the focusing phase is followed by a defocusing phase (see Figures 2, 4, or 6). During the defocusing phase of wave train evolution, ka decreases because of dispersion; nonlinear effects are weakened and should play only a minor role. If the duration of the focusing phase of wave train evolution is short compared to the time required for nonlinear effects to act, then nonlinear distortion of the wave train will be small. In contrast, in very weakly focusing, or nonfocusing (see Figure 8), wave trains, conditions conducive to the growth of nonlinear effects persist for a long time, so that these effects will eventually become important.

5. Summary and Discussion

Surprisingly, in our laboratory measurements on focusing unidirectional wave trains, nonlinear effects are stronger in deep water than in intermediate depth water and are stronger in nonfocusing wave trains than in focusing wave trains. These trends have been explained by the observation that the dominant source of nonlinear interaction in our measurements was the Benjamin-Feir instability, which acts only over a limited duration in focusing wave trains, only in wave trains whose bandwidth is narrow, and only in deep water. Under conditions in which the Benjamin-Feir instability does not act, linear theory predictions were shown to be in good agreement with measurements for wave trains with $(ka)_{\max}$ slightly in excess of 0.30 provided amplitude-dependent dispersion is taken into account.

Ocean waves are generally characterized by a spectrum with a broad distribution of energy in both angle and frequency. In deep water both of these properties preclude action of the Benjamin-Feir instability. (In finite depth water, however, a self-modulational instability of the Benjamin-Feir type may act on wave components that are not codirectional [*McLean*, 1982].) Thus conditions under which the Benjamin-Feir instability is able to act are expected to be satisfied only under extremely rare circumstances in deep water ocean waves.

Assuming this is true, our results have two important implications for deep water ocean waves. First, nonfocusing-induced extreme waves of the type observed in our group four experiments are expected to be extremely rare in deep water ocean waves. Indeed, we expect that the type of temporally limited action of the Benjamin-Feir instability that was observed in our groups two and three experiments is also rare in deep water ocean waves. Second, because the Benjamin-Feir instability apparently played no role in our group one experiments, we expect that the reported approximate limiting value of $(ka)_{\max}$ (below which a local linear theory description of the wave field is a good approximation) for these experiments (slightly in excess of 0.30) is most representative of deep water ocean waves. Thus there is reason to expect that a local linear theory description of non–locally-forced nonbreaking extreme waves in the ocean should be useful. Such a local description should not be expected to be accurate for times (distances) significantly in excess of a few tens of wave periods (wavelengths). Because the motivation for the work reported here was to understand the limits of validity of a linear theory description of wave fields in focal regions (which have limited spatiotemporal domains), we do not view this condition as a severe restriction.

Finally, we note that the extrapolation of our results on unidirectional waves to ocean waves should be questioned. Laboratory experiments on focusing waves in two horizontal directions should be performed to provide better insight into the dynamics of extreme ocean waves.

Acknowledgments. Discussions with John Grue and Mark Donelan and financial support from the Norwegian Research Council (for M.B. and A.J.) and the Division of Ocean Sciences of the U.S. National Science Foundation (for M.B.) are gratefully acknowledged.

References

Alber, I. E., The effects of randomness on the stability of two-dimensional wavetrains, *Proc. R. Soc. London*, *Ser. A*, *363*, 525–546, 1978.

Benjamin, T. B., and J. E. Feir, The disintegration of wave trains on deep water, part 1, Theory, *J. Fluid Mech*., *27*, 417–430, 1967.

Boccotti, P., On mechanics of irregular gravity waves, *Atti Accad. Naz. Lincei Mem. Cl. Sci. Fis. Mat. Nat. Sez. VIII*, *19*, 109–170, 1989.

Boccotti, P., A general theory of three-dimensional wave groups, part 1, The formal derivation, *Ocean Eng*., *24*, 265–280, 1997.

Brown, M. G., Space-time surface gravity wave caustics: Structurally stable extreme wave events, *Wave Motion*, *33*, 117–143, 2001.

Dias, F., and C. Kharif, Nonlinear gravity and capillary-gravity waves, *Annu. Rev. Fluid Mech*., *31*, 301–346, 1999.

Dommermuth, D. G., D. K. P. Yue, W. M. Lin, R. J. Rapp, E. S. Chan, and W. K. Melville, Deep-water plunging breakers: A comparison between potential theory and experiments, *J. Fluid Mech.*, *189*, 423–442, 1988.

Henderson, K. L., D. H. Peregrine, and J. W. Dold, Unsteady water wave modulations: Fully nonlinear solutions and comparison with the nonlinear Schrödinger equation, *Wave Motion*, *29*, 341–361, 1999.

Kennard, E. H., Generation of surface waves by a moving partition, *Q. Appl. Math*., *7*, 303–312, 1949.

Komen, G. J., L. Cavaleri, M. Donelan, K. Hasselman, S. Hasselman, and P. A. E. M. Janssen, *Dynamics and Modelling of Ocean Waves*, Cambridge Univ. Press, New York, 1994.

McLean, J. W., Instabilities of finite-amplitude gravity waves on water of finite depth, *J. Fluid Mech*., *114*, 331–341, 1982.

Mei, C. C., and P. F. Liu, The damping of surface gravity waves in a bounded liquid, *J. Fluid Mech*., *59*, 239–256, 1973.

Pelinovsky, E., and C. Kharif, Simplified model of the freak wave formation from the random wave field, *Proceedings of the 15th International Workshop on Water Waves and Floating Bodies*, edited by T. Miloh and G. Zilman, Dan Caesarea, Isr., 2000.

Phillips, O. M., D. Gu, and M. Donelan, Expected structure of extreme waves in a Gaussian sea, part I, Theory and SWADE buoy measurements, *J. Phys. Oceanogr*., *23*, 992–1000, 1993a.

Phillips, O. M., D. Gu, and E. J. Walsh, On the expected structure of extreme waves in a Gaussian sea, part II, SWADE scanning radar altimeter measurements, *J. Phys. Oceanogr*., *23*, 2297–2309, 1993b.

Pierson, W. J., M. A. Donelan, and W. H. Hui, Linear and nonlinear propagation of water wave groups, *J. Geophys. Res*., *97*, 5607–5621, 1992.

Rapp, R. J., and W. K. Melville, Laboratory measurements of deep water breaking waves, *Philos. Trans. R. Soc. London A*, *331*, 735–800, 1990.

Whitham, G. B., *Linear and Nonlinear Waves*, John Wiley, New York, 1974.

M. G. Brown, Rosenstiel School of Marine and Atmospheric Science, University of Miami, 4600 Rickenbacker Cswy., Miami, FL 33149, USA. (mbrown@rsmas.miami.edu)

A. Jensen, Mechanics Division, Department of Mathematics, University of Oslo, P.O. Box 1053 Blindern, N-1053 Blindern, N-0316 Oslo, Norway.

(Received August 7, 2000; revised April 3, 2001;
accepted April 27, 2001.)